

## Rapid Electronic Detection of Probe-Specific MicroRNAs using Thin Nanopore Sensors

Meni Wanunu,<sup>1\*</sup> Tali Dadosh,<sup>1\*</sup> Vishva Ray,<sup>1</sup> Jingmin Jin,<sup>2</sup> Larry McReynolds,<sup>2</sup> and Marija Drndic<sup>1</sup>

<sup>1</sup>*Department of Physics and Astronomy, University of Pennsylvania, Philadelphia PA*

<sup>2</sup>*New England Biolabs, Ipswich MA*

### Table of contents:

- SI-1.** Experimental details for fabricating different thickness SiN membranes
- SI-2.** AFM characterization of thinned SiN membranes
- SI-3.** Conductance of sub 10 nm thick nanopores as a function of time
- SI-4.** Geometric model for  $\Delta I$  of DNA as a function of effective pore thickness
- SI-5.** Scatter plots of  $\Delta I$  vs. transport time of 3 kbp DNA for two pore thicknesses
- SI-6.** Translocations of 10 bp DNA through a 3 nm diameter pore in a 7 nm thick membrane
- SI-7.** Discrimination among 25 bp DNA, 22 bp RNA, and 76-nucleotide tRNA
- SI-8.** Continuous traces for 25 bp DNA through a 3 nm pore for different voltages
- SI-9.** Continuous traces for 25 bp DNA at different concentrations
- SI-10.** Details of p19-based miRNA enrichment from cellular RNA extracts
- SI-11.** Continuous time traces of different concentrations of 22 bp RNA
- APPENDIX A.** Response of our system to artificial short current pulses

**SI-1. Experimental details for fabricating different thickness SiN membranes**

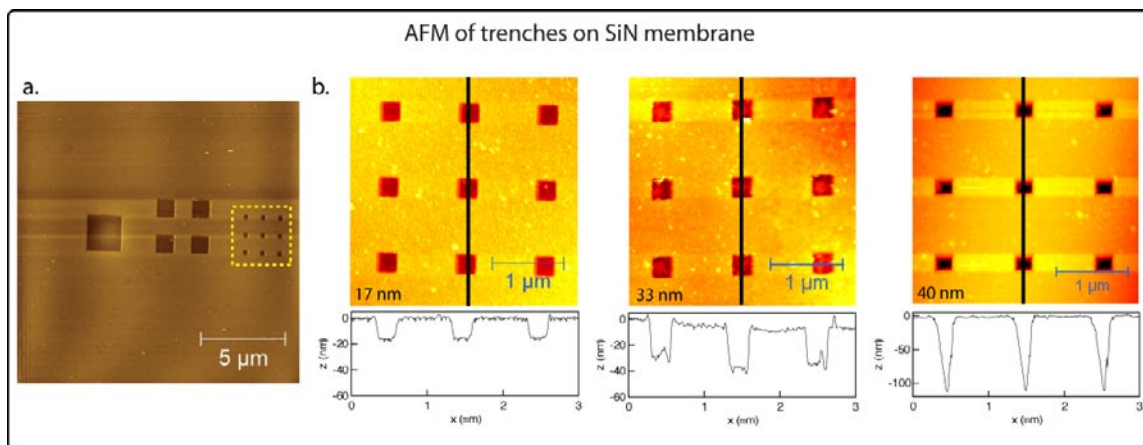
Sub-10 nm thick membranes were fabricated in  $5 \times 5 \text{ mm}^2$  Si chips that contain a  $5\text{-}\mu\text{m}$ -thick thermal  $\text{SiO}_2$  oxide underneath a 41 nm thick low-stress SiN layer, deposited by low-pressure chemical vapor deposition (Center for Nanoscale Fabrication, Cornell University). For characterization of the etch rate (see Figure 1c in manuscript) and for studying DNA transport through 60 nm thick membranes (see Figure 3 in the manuscript), we have used a different Si wafer that has a 100 nm thick SiN membrane. Prior to processing, the thickness of the SiN membrane was measured at different points on the Si wafer using a Rudolph Research AutoEL III Ellipsometer at a wavelength of 632.8 nm and an incidence angle of  $70^\circ$ . From the ellipsometric parameters, we obtained for the SiN film optical parameters of  $n = 2.24$ ,  $k = 0$ , as well as a film thickness of  $41.5 \pm 0.3 \text{ nm}$ . Standard photolithography followed by anisotropic KOH etch was used to produce a freestanding SiN membrane with approximate dimensions  $\sim 50 \times 50 \mu\text{m}^2$ . A subsequent buffered-oxide etch step was then performed to remove the  $5 \mu\text{m}$   $\text{SiO}_2$  layer from the KOH-etched side, in order to obtain freestanding SiN membranes. The SiN membrane was then spun-coated with a PMMA electron beam resist (a 2% solution of 950 kD molecular weight in chlorobenzene, MicroChem Inc.) followed by baking at  $180^\circ\text{C}$  for 10 minutes. Electron beam lithography was then used to write a pattern of squares with sides ranging from 250 nm to  $5 \mu\text{m}$ , using a 50 kV electron beam (Elionix 7500-ELS) and beam dose of  $750 \mu\text{C}/\text{cm}^2$ . The irradiated device was developed in 1:3 methyl isobutyl ketone:isopropanol volume ratio for 60 seconds followed by rinsing with isopropanol and drying under a stream of compressed nitrogen gas. Thinning of the exposed SiN areas was accomplished using a Technics PEIIA plasma etcher, using a 50W rf source and 400 mtorr  $\text{SF}_6$  chamber pressures. The SiN etch rate under these conditions was  $1.0 \pm 0.1 \text{ nm/s}$ . The resist was finally removed by  $\sim 1 \text{ h}$  incubation in warm acetone at  $65^\circ\text{C}$ , drying under a stream of  $\text{N}_2$ , and then heating at  $100^\circ\text{C}$  in hot piranha solution for 10 minutes (made by mixing 1:3 of 30%  $\text{H}_2\text{O}_2$  and conc.  $\text{H}_2\text{SO}_4$ )

[Caution: piranha is a strong oxidizer that reacts violently with most organic materials].

The chips were then washed with water, dried, and stored until use.

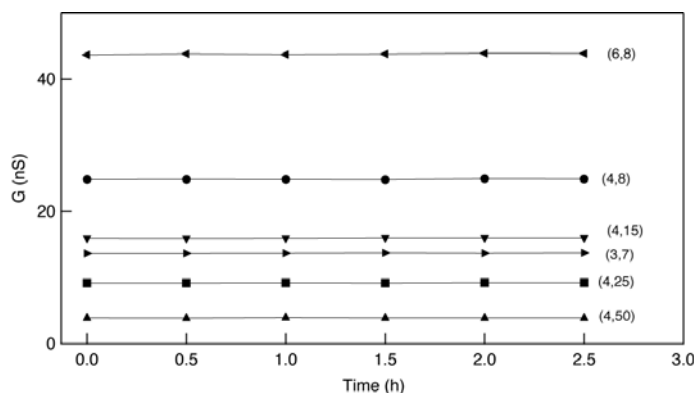
## SI-2. AFM characterization of thinned SiN membranes

Tapping-mode atomic force microscopy was carried out in order to characterize the process of localized membrane etching. All measurements were performed in ambient air using a Veeco EnviroScope to profile the etch depth and roughness of a given batch of processed chips. TESP Si tips (Veeco) with tip radii of  $<10$  nm were used for all images. In the Figure below, we show in panel (a) an AFM image of the pattern shown in Figure 1c of the paper, following a 17 nm etch process (the membrane curvature has been subtracted using a polynomial in order to improve visibility of the pattern). The dashed yellow line represents the  $3 \times 3$  array of  $250 \times 250$  nm squares that is shown in Figure 1c of the paper. In panel (b), three AFM images of 41 nm thick SiN windows in which a  $3 \times 3$  array of 250 nm squares with a  $1 \mu\text{m}$  pitch were plasma etched for 17, 33, and 40 seconds. Line profiles through a set of 3 squares can be seen below each image, showing step heights of  $17 \pm 1$  nm,  $33 \pm 1$  nm, and for the 40 nm thinning, the image shows a  $\sim 100$  nm deep triangular profile that resembles the tip shape, indicating that the membrane is completely perforated. The membrane thickness  $h$  in the processed region is given by the difference between the initial membrane thickness and the etch depth, i.e., in this case,  $h = 41 \text{ nm} - \text{etch depth}$ . We find that the minimum membrane thickness that is robust enough for experiments is a membrane that has been etched for 35 seconds, which yields a membrane thickness of  $\sim 6$  nm. Membranes with thickness values  $h \leq 5$  nm did not survive the piranha cleaning step.



**SI-3. Conductance of sub 10 nm thick nanopores as a function of time**

The figure below shows the conductance as a function of time for pores with various diameters  $d$  and membrane thicknesses  $h$ , denoted as  $(d, h)$ . The buffer used for all measurements was 1M KCl buffered to pH 8. Conductance values are reported in nS based on the current at 300mV and an electrolyte temperature of 21°C. The pores typically last for hours of use before requiring a cleaning step.



**SI-4. Geometric model for  $\Delta I$  of DNA as a function of effective pore thickness**

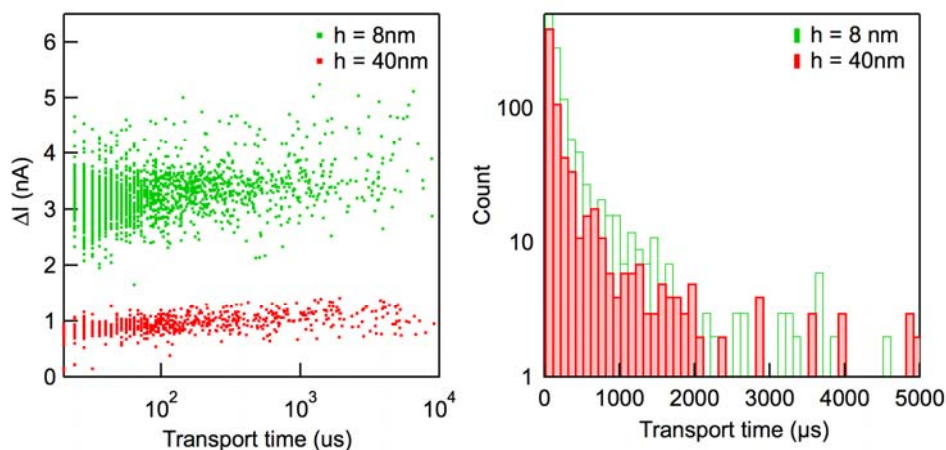
The expected values of  $\Delta I$  upon DNA entry were calculated based on *Equation 1* in the manuscript, with a modification that takes into account the displaced electrolyte current upon DNA occlusion of the pore. A hydrodynamic diameter for B-form DNA of 2.2 nm was assumed, as it was previously found to explain the observed relative conductance as a function of pore diameter  $d$  (see Ref. 41 in the manuscript). We express the current difference between an open pore  $I_o$  (see Eqn. 1 in main text) and a DNA-occluded pore  $I_{DNA}$  as:

$$\text{Eqn. 2: } \Delta I = I_o - I_{DNA} = I_o - V([\mu_K + (1-S)\mu_{Cl}]n_{KCl}e) \left( \frac{4h_{eff}}{\pi d_{eff}^2} + \frac{1}{d_{eff}} \right)^{-1}$$

where the two added parameters are  $d_{eff}$ , the effective pore diameter of the DNA-occluded pore (calculated from a circle of an equivalent area that is available for KCl transport in the case of the DNA occluded pore case), and  $S$ , the fraction of excluded  $\text{Cl}^-$  ions in the DNA-occluded pore. We model this exclusion of  $\text{Cl}^-$  ions as a coefficient from 0-1 that reduces the mobility of  $\text{Cl}^-$  ions (this is equivalent to a reduced  $\text{Cl}^-$  concentration). The rationale for chloride exclusion is based on previous results that showed an increase in  $\Delta I$  with DNA length for a length  $>1,200$  bp (see Ref. 41 in the manuscript), which we attribute here to a decreased effective concentration of anions (e.g.,  $\text{Cl}^-$ ) near the pore during translocation, due to electrostatic repulsion by the DNA coil. The red dashed line in Figure 2d is a best fit to  $\Delta I$  for a pore diameter  $d = 4$  nm as a function of the effective thickness  $h_{eff}$ , which yields values of  $d_{eff} = 2.83$  nm and  $S = 0.2$  (i.e., 20% exclusion of  $\text{Cl}^-$ ).

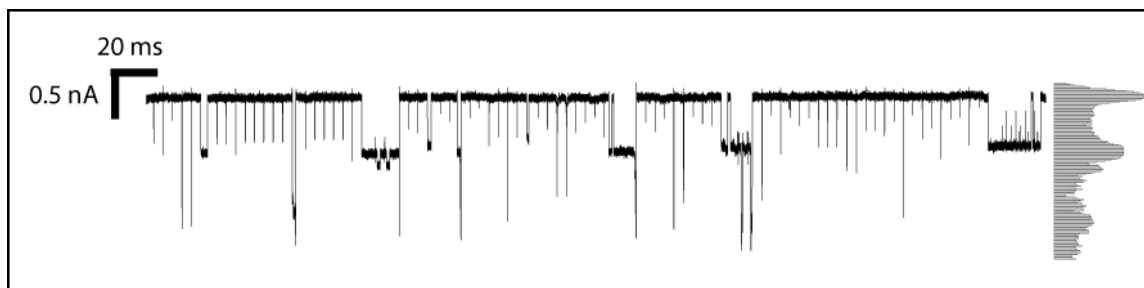
### SI-5. Scatter plots of $\Delta I$ vs. transport time of 3 kbp DNA for two pore thicknesses

The figure below shows a scatter plot of the mean current amplitude of each molecule ( $\Delta I$ ) and the total transport time for 3 kbp dsDNA through 4 nm pores as a function of membrane thickness ( $h$ ). Thinning the membrane has two observable consequences, one is increased  $\Delta I$ , which facilitates detection of the DNA, and the second is a minor decrease in transport times. Overall, transport times are only  $\sim 30\%$  smaller when reducing  $h$  from 60 to 6 nm, going from 0.95 ms to 0.72 ms. The plot on the right shows transport time distributions for two membrane thicknesses. Mean transport times are determined by fitting the distributions to exponentially decaying distributions, as described in Ref. 41.



### SI-6. Translocations of 10 bp DNA through a 3 nm diameter pore in a 7 nm thick membrane

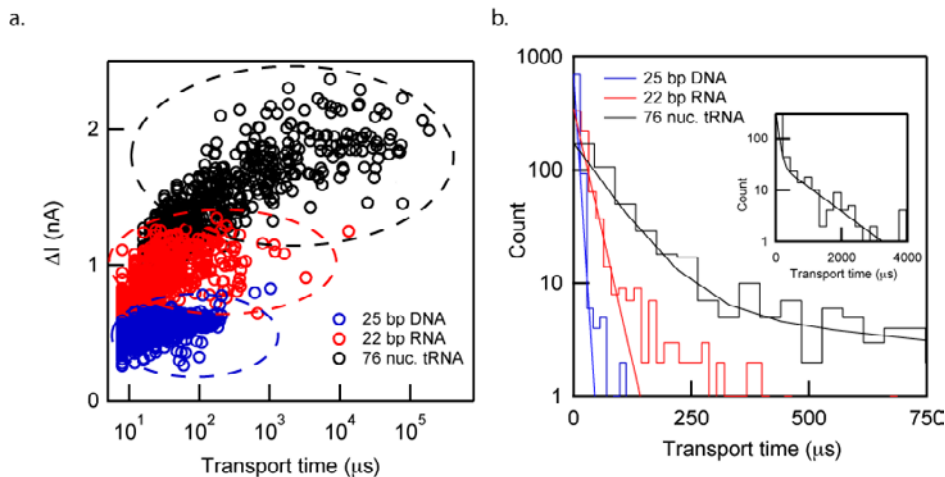
The figure below shows a set of 10 bp translocations through a 3 nm diameter pore in a 7 nm thick membrane under 500 mV applied voltage, at a temperature of  $0^\circ\text{C}$ . The events were concatenated by pasting together current spikes that include 2 ms current data before and after each spike. In contrast to events with the 25 bp DNA fragment, we consistently observe many deep and long events for the 10 bp sample, which was observed for many different 3 nm diameter pores. This may be attributed to sideways jamming of the molecule at the pore entrance, which would cause the DNA to stall for a relatively long time (milliseconds). The contour length of the 10 bp DNA is 3.5 nm, slightly higher than the pore diameter. An all-point histogram is shown to the right of the concatenated trace. The difference in amplitude between the first blockade peak and the open pore peak is 0.6 nA, similar to that of the 25 bp DNA sample (see Figure 4 in the manuscript). The second peak (1.1 nA) may be due to entry of two molecules simultaneously or sideways entry of the molecule into the pore. The traces for 25 bp DNA and the 22 bp RNA samples in Figure 4a of the manuscript show that such frequent blocking of the pore does not occur in double-stranded nucleic acids with contour lengths of at least 7 nm.



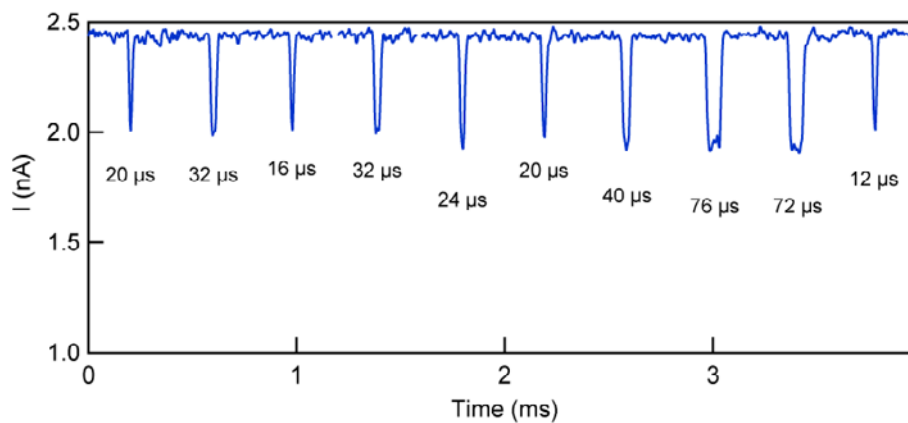
### SI-7. Discrimination among 25 bp DNA, 22 bp RNA, and 76-nucleotide tRNA

The following figure provides more detail about using a 3 nm diameter pore in a 7 nm thick membrane to discriminate among small nucleic acids of similar size, namely, 25 bp DNA (molecular weight = 15kD), 22 bp RNA (molecular weight = 15 kD), and 76-nucleotide tRNA (molecular weight = 25 kD). (a) Scatter plots of current amplitude ( $\Delta I$ ) vs. transport time for the three molecules under the same measurement conditions (0°C, 500 mV, 3 nm diameter pore in a 7 nm thick SiN membrane). The dashed ovals represent regions containing >85% of detectable events for each molecule type. (b) Transport-time distributions for >1,000 events of each molecule type. For the 25 bp DNA and 22 bp RNA, >90% of the data fits a single exponential decay, with timescales of 20  $\mu$ s and 50  $\mu$ s, respectively. On the contrary, for tRNA, the data fits a two-exponential function, with timescales 80  $\mu$ s and 1.04 ms (see inset of panel b for expanded view of the transport-time histogram for tRNA). While the short timescale may be due to collisions and fast translocations of the bulky tRNA molecule, the long timescale, in which the majority of events fall in, suggests that the tRNA must deform from its bent equilibrium structure in order to traverse the 3 nm diameter pore, a process that may stall transport, leading to longer dwell times and a broader dwell time distribution. Representative concatenated translocation events in the dwell time range of 12 – 228  $\mu$ s for 25 bp DNA (c) and 22 bp RNA (d). Events for the tRNA molecule are not shown here, because their duration is clearly longer, as seen in Figure 4a of the main paper. The corresponding transport times are noted below each event. These traces are shown in order to illustrate that the current amplitude for 25 bp DNA and 22 bp RNA are distinctly different, easily seen for events with duration longer than 30  $\mu$ s. These results suggest that the different amplitude spikes are a result of the different molecular properties between the three nucleic acids, rather than an artifact of fast dwell times close to the detection limit that would distort the current amplitudes. We note that the relationship between current amplitudes and

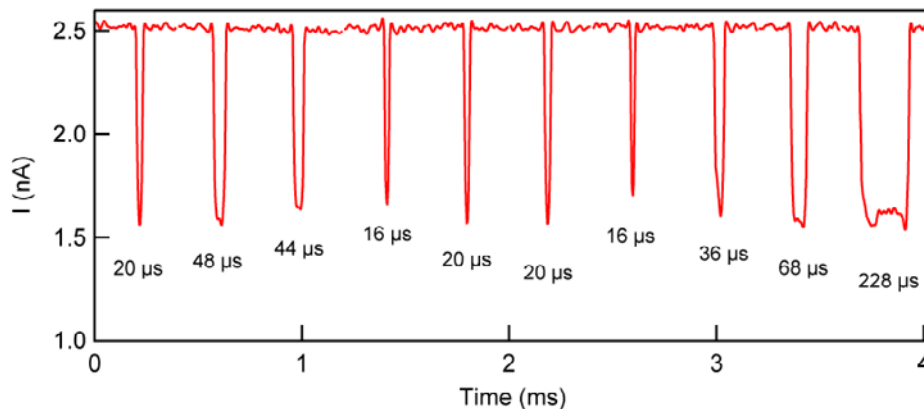
transport times in this study is not random, but rather expected if one considers the width/structure of the molecules: tRNA takes the longest to be transported because of its bent and bulky structure, while RNA takes longer to be transported than DNA because it is wider than DNA, which results in more extensive interactions with the 3 nm diameter pore. Bulkier structures will block more of the pore current, hence the link between increased current amplitudes and increasing transport times for the three molecules.



c. 25 bp DNA translocation events

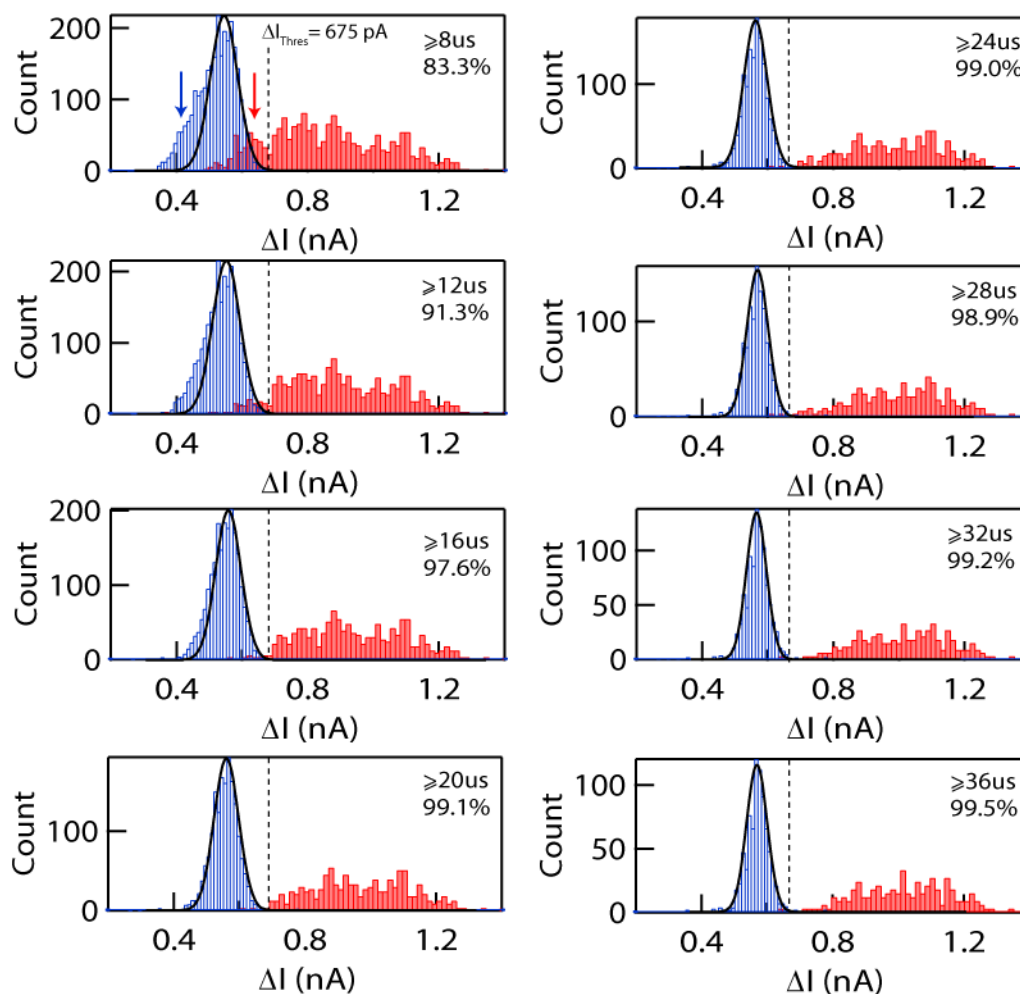


d. 22 bp RNA translocation events



A more quantitative analysis of our nanopore's ability to discriminate 25-bp DNA from 22-bp RNA based on current amplitudes is shown below. First, in order to test the response of our system to short pulses, we performed a simulation of ideal square current pulses with different durations and current amplitudes in the range 8 – 48  $\mu\text{s}$  (see APPENDIX A at the end of this document). The simulated events indicate that all events with durations  $< 20 \mu\text{s}$  are attenuated in terms of their amplitudes. For example, for pulse widths of 8  $\mu\text{s}$ , the mean attenuation factor is 20%. That is, events with 500 pA and 750 pA amplitudes are detected as 400 pA and 600 pA amplitudes, respectively.

Next, we show the effect of our rank 1 median filter on the real DNA and RNA data we collected for the scatter plots shown in the above Figure. We show below  $\Delta I$  distributions of for all the events in the scatter plots for 25-bp DNA (blue) and 22-bp RNA (red). In this series of histograms, we systematically take subsets of the dataset that contain events with duration equal to or longer than the indicated value in each plot.

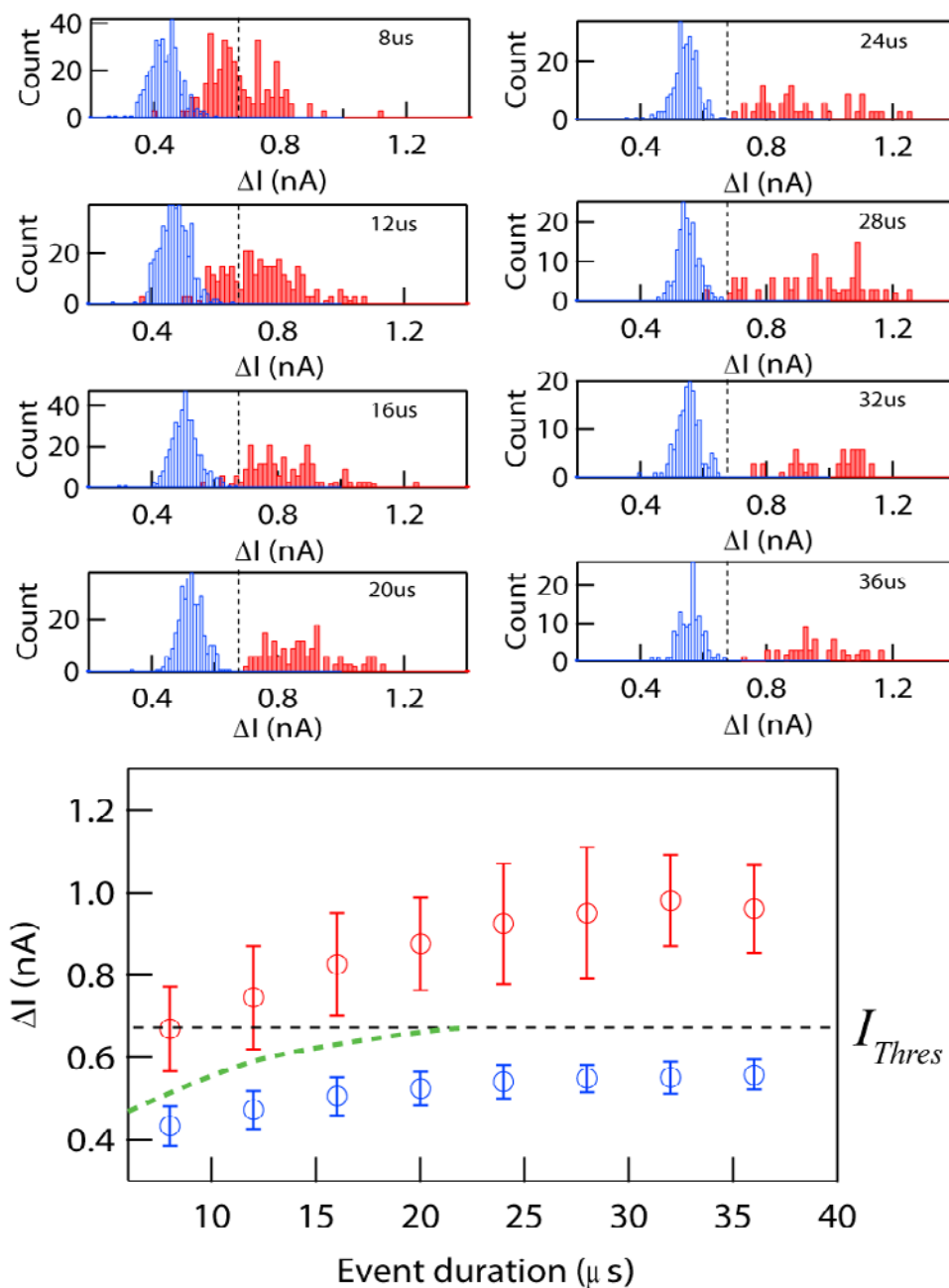


Also indicated in the plots are % certainty values for our discrimination between DNA and RNA, calculated from the fraction of RNA events that lie above the  $\Delta I_{Thres} = 675$  pA threshold (shown as dashed line). The threshold was chosen because <0.1% DNA events were found with larger  $\Delta I$  values. For example, including only events  $\geq 8$   $\mu$ s results in a certainty of 83.3%, because 16.7% of the RNA events have amplitudes that are lower than  $\Delta I_{Thres}$ . In other words, looking at all of our data in the range  $\geq 8$   $\mu$ s, we find that 16.7% of the RNA molecules are mixed with the DNA population, and therefore cannot be distinguished from DNA events. Now, when we only look at data  $\geq 12$   $\mu$ s, we find that 91.3% of the RNA events lie above the threshold, resulting in only 8.7% error in our discrimination. This certainty in our discrimination improves to >97% when only events  $\geq 16$   $\mu$ s are included. We note that events with durations  $\geq 16$   $\mu$ s constitute 75% and 73% of the total detected events for DNA and RNA, respectively. Finally, we note that differences in duration between DNA and RNA cannot explain the differences in current amplitudes, because events longer than 36  $\mu$ s, which represent about one half of the datapoints, have a clear plateau at the mean current amplitude value, unequivocally showing that DNA and RNA provide distinguishable current amplitude levels.

We also point out that our bandwidth-limited data acquisition results in asymmetric shapes for the current amplitude distributions, which exhibit “bellies” or “shoulders” at 0.4 nA and 0.6 nA for DNA (blue arrow) and RNA (red arrow), respectively. These “bellies”, which clearly deviate from expected Gaussian shapes (see black curves), disappear completely for events with durations of  $\geq 16$   $\mu$ s, and the distribution shapes are Gaussian thereafter. From the simulations shown in Appendix A, this asymmetry is clearly a result of attenuation by our filter.

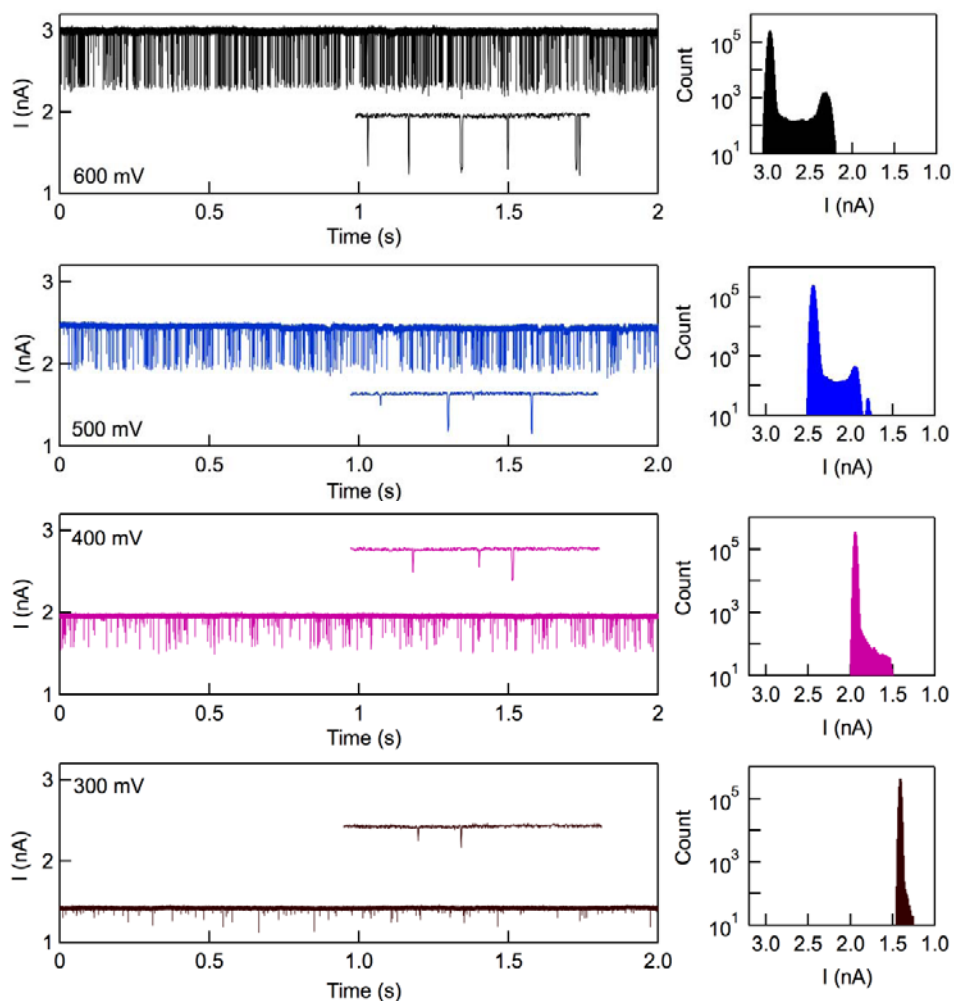
However, despite the signal attenuation, we still can discriminate among short DNA and RNA, provided that we choose the correct threshold amplitude for discrimination that considers the event duration. To illustrate this, we show on the next page  $\Delta I$  histograms for DNA and RNA events where in each plot we analyze slices of the data that select all events with an indicated duration, in the range of 8-36  $\mu$ s. In each plot we draw the dashed line for  $\Delta I_{Thres} = 675$  pA as a guide to the eye. Below all the distributions, we plot the mean  $\Delta I$  values as a function of event duration (the error bars show one standard deviation in each direction). As seen in these plots, the current amplitude signals for *both*

RNA and DNA are distorted towards lower  $\Delta I$  values for events in the range 8-16  $\mu\text{s}$ , after which there is no apparent shift in the position of the distributions. The magnitude of this distortion for short events is up to 150 pA for the 8  $\mu\text{s}$  events (or 22% of the  $\Delta I$  value), in good agreement with the simulated data. The attenuation factor appears robust as a function of event duration, and therefore in our discrimination we can compensate for attenuated data by adapting the threshold (see green dashed line in the plot below), in order to discriminate DNA from RNA in this regime with >90% confidence.



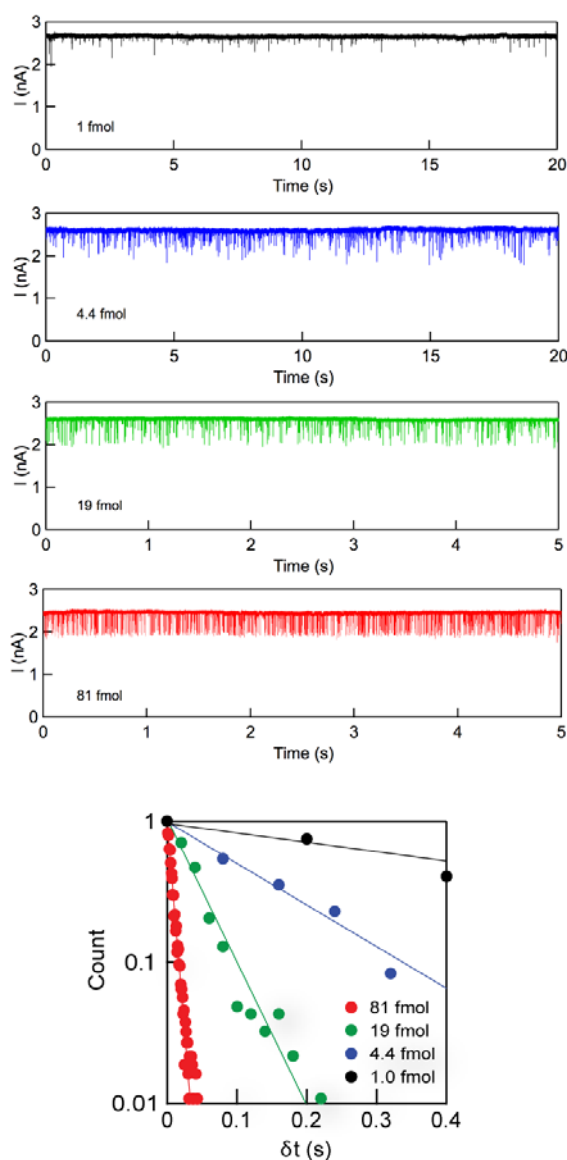
**SI-8. Continuous traces for 25 bp DNA through a 3 nm pore for different voltages**

The figure below shows 2-second current traces under different applied voltages of a 25 bp DNA sample analyzed using a 3 nm diameter pore fabricated in a 7 nm thick membrane (data taken at a temperature of 0°C). The analyte chamber contains 25 bp DNA at a concentration of 81 fmol/μl, and positive voltage is applied to the second chamber in order to drive DNA to the other side. The inset trace in each plot is a zoomed-in 7 ms view, with the same current amplitude scale as the y-axis. On the right, all-point current histograms are shown for each trace. Increasing the voltage greatly increases the capture rate, as seen by the increasing amount of deep events. The shallow events for the low voltage traces are presumably collisions of the DNA with the pore. The fraction of these collisions decreases with increasing voltages, in line with a voltage-activated barrier for threading (see manuscript text).



### SI-9. Continuous time traces for 25 bp DNA at different concentrations

The figure below shows current vs. time traces for a 3 nm diameter pore at a measured at a voltage of 500 mV and a temperature of 0°C, when different concentrations of DNA were added to the pore (expressed as fmol/μl solution). While the open pore current remains similar for different concentrations of DNA (~2.5 nA), the number of spikes increases as a function of the concentration, as expected. The rate of events shown in Figure 3d were derived from the time-delay distributions ( $\delta t$ ) between two successive events (see plot below the traces), which fits a first arrival time distribution function  $P_{capture} = A \exp(-Rate * t)$ , where the slope of the exponent (i.e., *Rate*) is the mean capture rate in  $s^{-1}$ .



**SI-10. Details of p19-based miRNA enrichment from cellular RNA extracts**

The p19 protein binds tightly to double-stranded RNA that is 19 to 22 basepairs in length. There is no binding to single stranded RNA. This tight, selective binding of p19 to dsRNAs allows the enrichment from cellular RNA of probe-hybridized miRNAs that have a very low abundance. For example, miR153, a miRNA with very low abundance compared to other miRNAs, has been enriched by over 100,000-fold from cellular RNA (see Ref 54 in the manuscript).

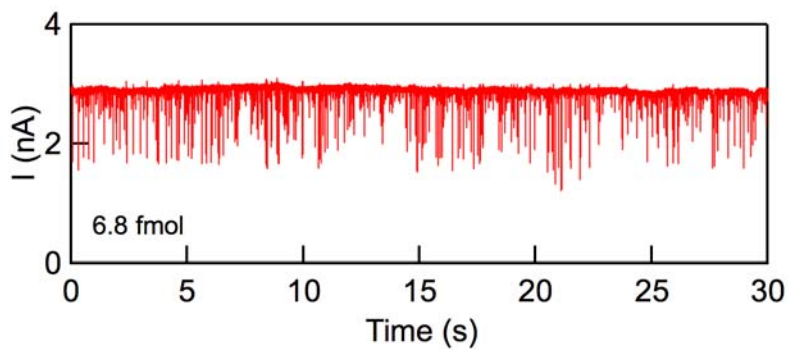
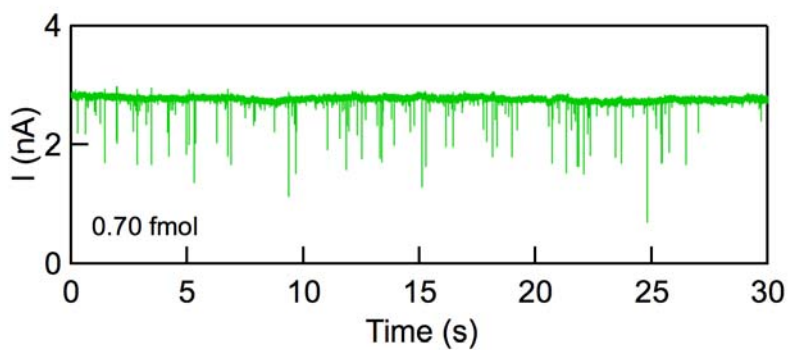
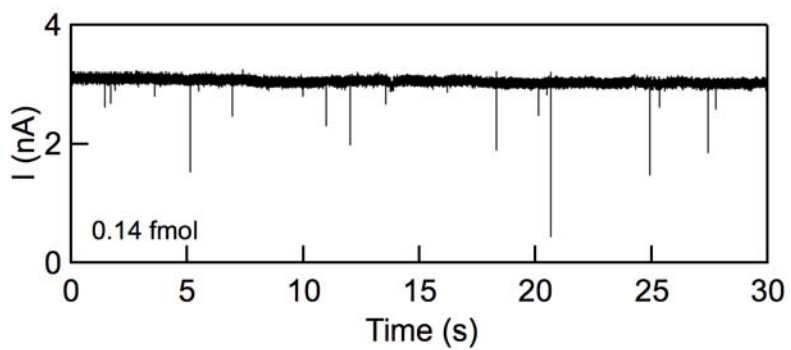
The protocol of miRNA enrichment proceeds as follows: A synthetic 22 nucleotide RNA oligo probe of sequence 5'-AACACCAUUGUCACAC-UCCAUA-3' (Integrated DNA technologies, Inc.) complementary to miR122a was first phosphorylated at the 5' end using T4 polynucleotide kinase (New England Biolabs, Ipswich, MA). The miR122a-specific probe was then added to PCR tubes containing the different RNA samples (rat liver RNA, positive control, and the four negative controls) in 1X p19 binding buffer (20 mM Tris-HCl, pH 7.0, 1 mM EDTA, 1 mM tris (2-carboxyethyl) phosphine, 100 mM NaCl, 0.02% Tween-20) in a total volume of 10  $\mu$ l. Hybridizations were carried out in a thermal cycler programmed to 75°C for 5 min, followed by 52°C for 5 hours. Each 10  $\mu$ l of hybridization reaction was incubated with 10  $\mu$ l of p19 beads suspended in 1X p19 binding buffer, 10 units of murine RNase inhibitor (NEB), and 1 mg of BSA in a total volume of 20  $\mu$ l. The binding reaction was incubated by shaking for 1-2 h at RT in an Orbis shaker (MarketLab, Caledonia, MI, USA). Using a magnetic rock (NEB), the unbound RNA was removed by washing 6 times in 600  $\mu$ l of 1X p19 wash buffer (20 mM Tris-HCl, pH 7.0, 1 mM EDTA, 100 mM NaCl). For each wash, the beads were shaken for 5 min. at 37°C on a heated shaker. After the third wash, the washing temperature was increased to 42°C to remove all of the non-specific unbound RNA. The probe:miR122a duplex was eluted from the p19 beads into 20  $\mu$ l of 1X p19 elution buffer (20 mM Tris-HCl adjusted to pH 7.0, 100 mM NaCl, 1 mM EDTA and 0.5% SDS) by shaking for 20 min at 37°C. SDS was removed by adding 16  $\mu$ l of 4 M KCl to the 160  $\mu$ l

eluate and cooling to 4°C. After centrifugation for 15 min. at 14,000 rpm in a microfuge, the solution was carefully decanted to a new tube to remove the white SDS pellet. The isolated miRNA were diluted into KCl solutions such that the total KCl concentration was 1M, and the solution was added to a 3 nm diameter nanopore in a 7 nm thick membrane for detection, which was carried out for all samples at 0°C and 500 mV.

The sequence of experiments that led to the data for Figure 5 is as follows: A calibration curve for different 22 bp duplex RNA concentrations was first performed using the synthetic probe:miR122a duplex, after which the negative controls **NC1-NC4** were tested, and finally, samples **RL** and **PC** were tested. Between each sample, the chamber was rinsed 10 times by removing the chamber contents, adding 20 µl of fresh buffer, mixing the chamber contents using a pipette, and repeating the process. After each cleaning procedure, a 20 second trace was collected to verify that the baseline current was within 5% of the open pore current value, and that no detectable events are present. During data acquisition for the negative controls, evidence that the nanopore is active comes from the fact that we did occasionally observe shallow events (<0.3 nA), which we attribute to trace amounts of single-stranded RNA (e.g., the hybridization probe) present in the p19-treated samples.

### **SI-11. Continuous time traces of different concentrations of 22 bp RNA**

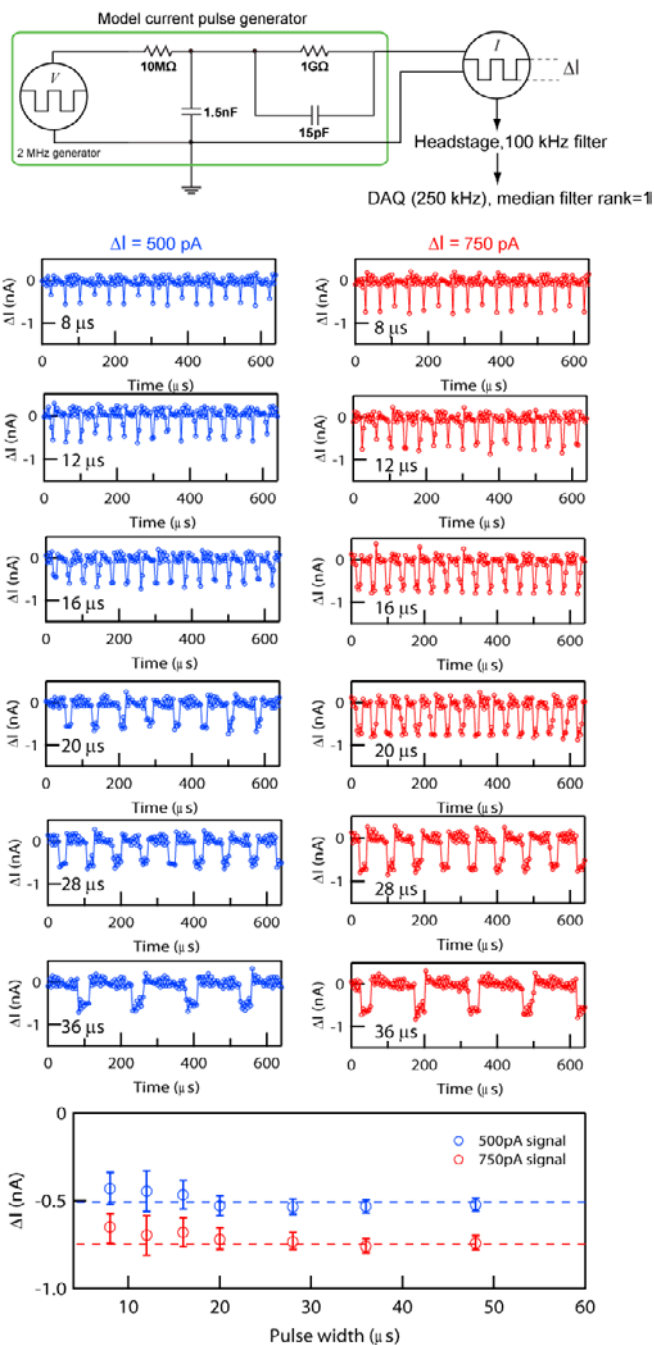
The figure below shows continuous time traces for a 3 nm diameter pore measured at a voltage of 500 mV and a temperature of 0°C, when different concentrations of RNA were added to the pore (expressed as fmol/µl solution). The calibration curve in Figure 5c of the paper was constructed by calculating for each trace the mean capture rate as a function of the RNA concentration.



## APPENDIX A: Response of our system to artificial short current pulses

In order to test our system's response to very fast translocation events we tested the response of our amplifier to synthetic current pulses in the range 8 – 48  $\mu\text{s}$ . The scheme for generating these pulses is shown below: A 2 MHz square wave generator with asymmetric pulse capabilities (TENMA Jupiter 2010) was fed into the compensated RC circuitry shown in the Figure below.

The circuitry converts the voltage signal of the generator into a current pulse train with specified durations and amplitudes, adjusted manually by reading the function generator's output using an oscilloscope. Next, we generated current pulses of durations in the range 8 – 48  $\mu\text{s}$ , fed the signal into our amplifier's headstage, then digitized the output at a sampling rate of 250 kHz using a DAQ card and median filtered our data using a rank of 1. Combined with the 100 kHz bandwidth of the Axopatch 200B patch clamp amplifier, which is set by its internal 4-pole Bessel filter<sup>1</sup>, a rank 1 median filter behaves as a low-pass filter with a corner frequency of  $f_c=37.8$  KHz at 250 kHz sampling rate. The roll-off of this median filter is shallower than commercial low-pass filters. Representative traces are shown for



<sup>1</sup> Axopatch 200B Patch Clamp: Theory and Operation", Rev D, Axon Instruments, Foster City, CA, 1999), page 63.

pulses of the indicated durations and two amplitudes,  $\Delta I = 500$  pA (blue) and 750 pA (red), which model events from the short DNA and RNA molecules, respectively. A plot of the mean  $\Delta I$  values vs. pulse duration shows that events of duration  $\leq 20$   $\mu$ s are attenuated. However, the attenuation factor is similar for the 500 pA and the 750 pA pulses: for the 8  $\mu$ s pulses that are detected as a single sample point, the *peak* amplitude was attenuated by 14% for both pulse amplitudes.

**Acknowledgement:** We sincerely thank Winfield Hill and Ken Healy for helpful advice on designing the RC circuitry.